Mobilized lateral earth pressure coefficient (K_{mob}) in peat under staged road embankment loading

Alsidqi Hasan[1,2*], *Jeffery G.K.* Tay[2], *Cassidy* Morris[3], and *Lin Jye* Lee[3]

[1] Department of Civil Engineering, Universiti Malaya, Kuala Lumpur, Malaysia
[2] Department of Civil Engineering, Universiti Malaysia Sarawak, Kota Samarahan, Malaysia
[3] Sarawak Public Works Department, Kuching, Malaysia

Abstract. This paper presents a preliminary analysis of the mobilized lateral earth pressure coefficient (K_{mob}) of peat under staged road embankment loading. Data were obtained from a Category 5 rural primary road (R5) project in Malaysia using a novel Subsurface Sensor Module (SSM). The SSM integrates orthogonally installed earth pressure cells, a piezometer, and a settlement gauge within the central peat layer, providing high-frequency digital measurements at 10-minute intervals. These data are complemented by manual settlement plate measurements, inclinometer readings, and extensometer data. In this study, K_{mob} is defined as the mobilized ratio of effective horizontal stress to effective vertical stress beneath the embankment centerline. Findings reveal that K_{mob} is not bounded between K_a and K_p as conventionally assumed; instead, it originates in an unstable state ($K_{mob}<K_a$), evolves through K_a and K_o, and ultimately trends toward K_p. Observations beneath the centerline indicate that the peat undergoes lateral strain; thus deviating from the pure K_o compression conditions typical of standard oedometer testing. Instead, K_{mob} follows a specific stress-path-dictated evolution spanning K_a to K_o before transitioning into a passive loading state where K_{mob} approaches K_p. Results indicate that monitoring K_{mob} serves as a critical real-time indicator of embankment stability. This approach allows engineers to optimize construction protocols regarding filling sequences and rest periods, thereby enhancing efficiency and timelines. Integrating stress sensors with standard instrumentation provides the high-fidelity data necessary for rigorous analysis and field management. These findings offer valuable insights for the optimal design of road embankments on peat.

1 Introduction

The expansion of transportation infrastructure across peat deposits remains one of the most difficult challenges in the current geotechnical engineering practice. Peat has exceptionally high natural water content, low undrained shear strength, and significant secondary compression (creep). Therefore, the road embankment construction on peat deposits necessitates specialized mitigation strategies to ensure stability and limit long-term deformations; among these, staged construction is recognized as a primary approach [1,2]. While the primary objective of the staged loading is to facilitate a controlled increase in effective stress and shear strength through consolidation, the evolution of the lateral stress state during this process remains a critical, yet frequently oversimplified and marginalized, design parameter.

The mobilized lateral earth pressure coefficient (K_{mob}) is fundamental to the stability and the serviceability of the embankment. Unlike the static coefficients traditionally employed for limit-state analyses (i.e. K_a, K_o and K_p), K_{mob} captures the transient effective stress ratio as the soil skeleton evolves from an initial to the final state of embankment loading.

Within the context of this study, K_{mob} is defined as:

$$K_{mob} = \frac{\sigma'_h}{\sigma'_v} \tag{1}$$

where σ'_h and σ'_v represent the mobilized horizontal (lateral) and vertical effective stresses, respectively, developed during the embankment loading and subsequent consolidation phases.

The understanding of how lateral pressure evolves from an at-rest (K_o) state toward a limit state (active, K_a or passive, K_p) was pioneered by Clough and Duncan [3]. Their work established that the mobilization of earth pressure is strictly a function of soil-structure displacement, proving that the lateral earth pressure coefficient is not a static constant but a transitional variable dependent on the magnitude and direction of soil movement. In the context of peat, this transition is further complicated by the peat's fibrous anisotropy and unique time-dependent characteristics [4,5]. As noted by Duncan and Seed [6], the stress history and the specific path of loading play a decisive role in the resulting lateral pressures. This is particularly relevant in staged loading, where pore water pressure dissipation and soil solids rearrangement occur incrementally over time. Inaccurate estimation of K_{mob} can lead to the lateral squeezing phenomenon, inducing unanticipated bending

* Corresponding author: alsidqi_hasan@yahoo.com

moments and shear forces in adjacent infrastructure, such as bridge piles or buried culverts. The good estimation can be useful for effective design of counterberms (act as dead weight that resists the lateral thrust and prevent heaving), monitoring stability during construction, and better accuracy in settlement prediction using modern numerical model such as finite element method.

While widespread adoption of advanced Finite Element Method (FEM) software has incorporated the non-linear soil-structure interaction principles originally framed by Clough and Duncan [6], a distinct gap remains in the literature regarding the temporal evolution of K_{mob} during the intermittent rest periods of staged construction on peat ground. Current research highlights that although vertical settlements are well-documented, the horizontal stress change resulting from the soil relaxation, the unloading and reloading, require more thorough investigation [7].

This paper addresses this gap by investigating the evolution of the mobilized lateral earth pressure coefficient in peat under staged road embankment loading. Utilizing the state-of-the-art field instrumentation, this study tracks the temporal variations of K_{mob} during construction of a staged embankment. The findings bridge the gap between classical earth pressure theory and modern infrastructure challenges, providing a refined basis for the design of resilient transportation networks on problematic peat ground.

2 Subsurface profile

The evolution of K_{mob} is being investigated as part of a comprehensive monitoring program for a road embankment on peat, currently under construction in Sarawak, Malaysia. The study area is situated at global coordinates 1°21'58.9"N and 111°08'04.4"E, a region characterized by extensive peat and alluvial deposits.

Fig. 1 illustrates the subsurface profile at a representative transverse section at chainage CH 26+600, located within the 100m road segment extending from chainage CH 26+550 to CH 26+650. The stratigraphy was characterized through an integrated site investigation (SI) comprising four Peat Auger (PA) samplings and a Standard Penetration Test (SPT) borehole. The SI was performed after site clearing and prior to any loading imposed to the soil.

The subsurface primarily consists of distinct layers of peat and silt, with a relatively uniform interface and an average peat depth of 4.9 m. Due to the high compressibility and low resistance of the organic material, the SPT yielded N-values of zero throughout the peat profile, as the material yielded under the static weight of the hammer and drill rods. To supplement these findings, Field Vane Shear (FVS) tests were conducted to evaluate both undisturbed (FVS-U) and remolded (FVS-R) shear strengths. These tests revealed an undrained shear strength (s_u) of up to 32 kPa, providing a more reliable characterization of the peat's initial consistency.

Table 1 summarizes the physical and mechanical properties of the peat and silt samples obtained during the SI (prior to any loading). The peat can be classified as H_7 (Sapric) according to von Post scale [8] and is underlain by elastic silt with a Plasticity Index (PI) of 50. A thin transitional zone exists at the boundary between the peat and silt, where the silt contains a noticeable amount of sand. It is important to note that the peat's organic matter is below the 75% by dry-weight threshold required by ASTM D4427 [9]. However, it satisfies the classification criteria of other established systems. For instance, the USDA system requires a minimum of only 16.5% organic matter, while the Russian system sets the threshold at 50% [10,11]. The organic matter of the peat is within the range of East Malaysian peat, i.e. between 50%-98% [12]. Consequently, for the scope of this study, the material is characterized as peat.

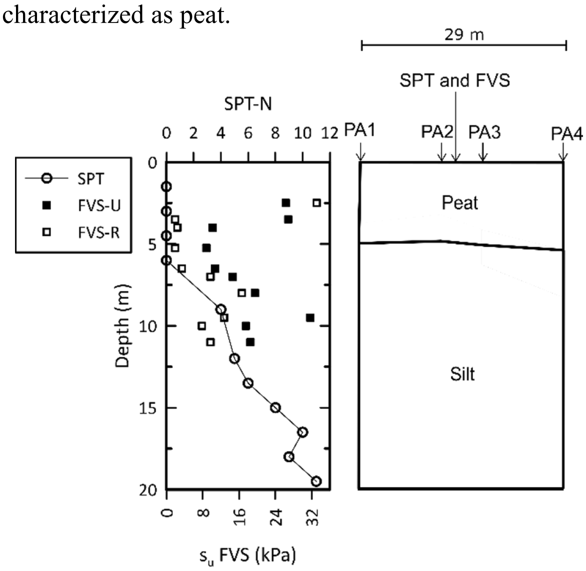

Fig. 1. Subsurface profile.

Table 1. Physical and mechanical properties of the subsurface.

Properties	Values/ Characteristics
Peat	
G_s	1.78
Von Post scale	H_7
Color	Dark brown
In-situ moisture content (%)	460.5
Organic matter (%)	55.3
Fiber content (%)	14.4
ϕ' (°)	16.1
Silt	
G_s	2.68
ϕ' (°)	14.4
c' (kPa)	6.6
LL	99
PL	49

3 Field instrumentation

This study utilizes a specialized Subsurface Sensor Module (SSM), a custom-engineered apparatus designed to integrate high-precision electrical sensors within a lightweight, stainless-steel frame. This module is engineered to minimize disturbance during installation while maintaining the structural integrity required to secure the sensors in place (Fig. 2). The frame, measuring 500 mm × 450 mm × 940 mm, secures the sensors via mechanical fasteners and high-tensile cable ties. The fully assembled module reaches a total mass of roughly 28 kg, exerts a self-weight stress of approximately 1.2 kPa.

The SSM was deployed within the center of the peat layer using a burial method facilitated by a temporary steel casing. Sensor cables were routed to a data logger positioned several meters away from the active construction area above ground. The installation methodology aligns with Hasan et al. (2023) [13], though the original instrumentation in that study was deployed at a separate location.

Fig. 2. Subsurface Sensor Module (SSM).

The SSM incorporates a specific assembly of sensors designed for stress-strain monitoring:

1. Two units of Vibrating Wire Earth Pressure Cells (EPC1 and EPC2). The EPC1 is axially mounted circular plate, measures total vertical stress. The EPC2 a flat circular plate measures total horizontal stress. Each plate surface is oriented to directly face the principal direction, i.e. y-axis (horizontal axis in the cross section) and z-axis (vertical) of the stress being measured.
2. One unit of Vibrating Wire Piezometer (PZ). The PZ, is oriented vertically within the frame to monitor pore water pressure. The PZ1 is positioned at the same level as the earth pressure cells to provide correlated pressure and stress data.
3. One unit of Vibrating Wire Settlement Gauge (SG). The SG is mounted horizontally on the top surface of the SSM frame to monitor vertical displacement. The gauge is connected via a fluid-filled tube to an above-ground reservoir located 35 m from the road centerline. The reservoir is mounted on a pile that was driven firmly into the underlying hard soil layer. The reservoir (fixed on pile) serves as the stable reference datum. As the SSM settles, the pressure change in the fluid column is measured by the vibrating wire sensor, establishing a reliable baseline for displacement readings.
4. Electric Biaxial Tiltmeter (TM). The TM monitors the orientation of the SSM frame by providing tilt angles along two orthogonal horizontal axes: the x-axis (parallel to the chainage) and the y-axis (perpendicular to the x-axis, i.e. cross section).
5. Electric Magnetic Compass (MC). The MC measures the rotation (azimuth) of the SSM frame about the z-axis, referenced to magnetic North. The MC was used for short-term operational use during deployment of the SMM.

In addition to the SSM, a settlement plate, an inclinometer, and an extensometer system were installed at the center of the road embankment. The settlement plate monitors ground surface settlement and embankment fill height via its riser pipe. Simultaneously, the extensometer system tracks movement across eight distinct soil layers via its “spider magnet” sensors, focusing particularly on the interface between the peat and silt.

The SSM and the supporting instrumentation were installed and ready to be used approximately two months before the commencement of embankment construction. This lead time was established to ensure baseline stabilization and allow for the rectification of any potential malfunctions. However, all instruments performed as expected throughout the pre-construction phase.

4 Monitoring

Fig. 3 illustrates the embankment cross-section 818 days (approximately 27 months) post-installation, corresponding to 756 days (approximately 25 months) after the commencement of construction. The hatched area denotes the compacted fill, which is currently situated both above and below the original ground level (O.G.L.) due to settlement. As of the time of writing, filling operations remain ongoing, with a target finished road level set at 2.95 m above the O.G.L. The road features a total surface width of 15 m, consisting of a 7 m central paved carriageway with a 2 m paved shoulder and a 2 m unpaved shoulder provided on both sides. To enhance embankment stability, 1 m high counterberms were constructed on both sides, bringing the total width of the cross-section to 45 m. Side slopes for both the embankment and counterberms follow a 2H:1V ratio. For drainage, the road surface and counterberm surfaces maintain transverse gradients of 2.5% and 2%, respectively.

For basal reinforcement, a double layer of woven geotextile (Type 85, with a tensile strength of 85 kN/m) was installed at the interface between the embankment fill and the natural ground. Notably, the design did not incorporate vertical drains.

The design specifies embankment filling in 300 mm increments (lifts), each followed by a two-week rest period, with the exception of an initial 500 mm drainage layer (blanket). The drainage layer used compacted sand and wrapped between the double layer geotextile. All layers, including the drainage blanket, were compacted to a target unit weight of 18 kN/m³. While the drainage layer was strictly comprised of sand, the subsequent embankment lifts utilized either sand or suitable selected fill. Due to frequent construction delays, the as-built elevation at the centerline reached only 1.375 m above the O.G.L. at 25 months post-commencement, as represented by the hatched area in Fig. 3. Only 38% of the total fill volume remains above the O.G.L. as an effective embankment, while the remaining 62% has settled below the original ground level, contributing to the submerged portion of the fill. The total height of the fill at the center of the embankment (both above and below the O.G.L.) is 3.87m.

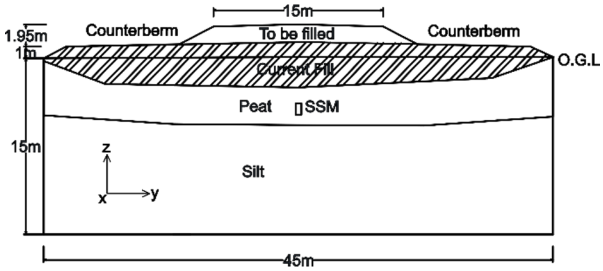

Fig. 3. Embankment and the current fill.

Ground settlement was determined via settlement plate readings, while the vertical compression of the peat and silt layers was monitored using the extensometer system. Data from the extensometer indicated that the silt layer at a depth of 15 m underwent negligible settlement, suggesting that the current fill load does not induce deformation in soil strata deeper than 15 m. Table 2 summarizes the total ground settlement and the respective deformation of the peat and silt layers at the centerline after 25 months.

Table 2. Ground settlement and peat deformation at the centerline.

Settlement and Deformation	(m)
Ground surface settlement	2.38
Peat-silt boundary settlement	0.76
SSM settlement	1.92
Inital peat thickness at the centerline	4.86
Current peat thickness (after compression)	3.22
Peat deformation (compressed)	1.68
Silt deformation (compressed)	0.8

Fig. 4a presents the total vertical stress, total horizontal stress, and pore water pressure obtained from the EPC1, EPC2, and PZ sensors in the SSM, respectively. Monitoring data from the SG sensor shows that the SSM experiences settlement in direct response to the increasing vertical stress of the embankment (Fig. 4b). However, the TM sensor recorded negligible tilting with respect to both the x- and y-axes. Consequently, the measurements from EPC1, EPC2, and SG do not require tilt correction.

The spikes in total stress and pore water pressure indicate the stage-filling phases, while the subsequent dissipation curves represent consolidation. Two significant spikes are observed: the first occurred during the initial 500 mm lift (which exceeded the specified 300 mm), and the final spike resulted from a non-conformance activity. In the latter instance, the contractor placed a 1 m fill layer, bypassing the filling rate specifications. Consequently, the fill was trimmed back to 300 mm following the issuance of the non-conformance report. The settlement measurements reflect the embankment loading; as the load increases, settlement increases proportionally. However, some rebounds are visible in the settlement curve, which are attributed to heaving caused by filling activities at the sides of the embankment.

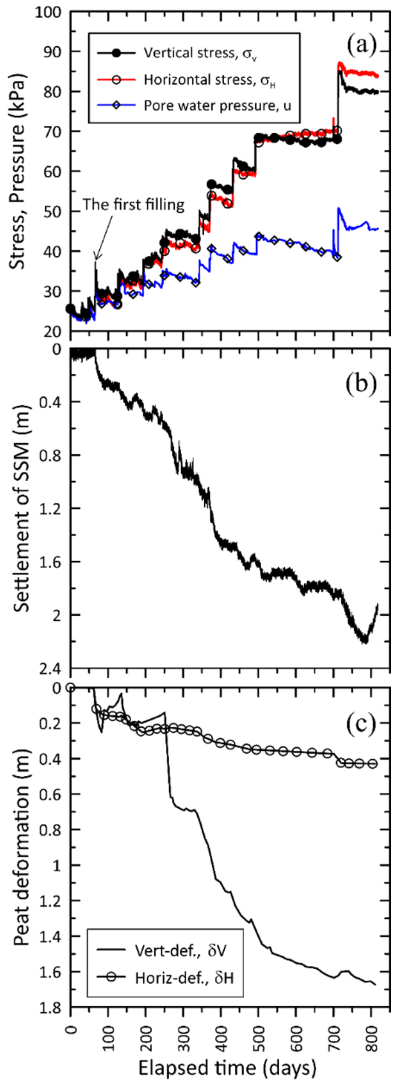

Fig. 4. Data monitoring (a) stresses and pore water pressure, (b) settlement of the SSM, and (c) peat deformations.

Fig. 4c illustrates the peat deformation, specifically the reduction in peat thickness, *δV* (m) and the horizontal deformation, *δH* (m), plotted against elapsed time. The reduction in thickness was calculated by subtracting the settlement at the peat-silt boundary (obtained via the extensometer spider magnet) from the original ground level settlement (obtained via the settlement plate). Meanwhile, the horizontal displacement was monitored by the inclinometer (located at the center of the embankment); measurements were taken at the specific depth of the SSM, which evolved over time as the peat layer underwent compressed. The vertical deformation of the peat is significantly higher, approximately four times greater than the horizontal displacement. The most rapid reduction in peat thickness occurred around day 250, coinciding with the peak filling activity when the monthly filling rate was at its highest. This steep reduction in thickness is also reflected in Fig. 4b, where the SSM settlement curve reaches its maximum gradient.

The rate of reduction in peat thickness stabilizes around day 500, following a 300 mm fill increment and a subsequent extended rest period due to construction delays. Contrary to conventional assumptions, primary consolidation in the peat appears to occur relatively rapidly. This behavior may be partially attributed to the high initial permeability of Sapric peat; however, laboratory tests indicate that this permeability eventually diminishes over time due to clogging mechanisms within the soil structure [14].

The monitoring data presented in Fig. 4 provides the empirical basis for the K_{mob} analysis discussed in the subsequent sections.

5 Evolution of K_{mob}

The effective vertical and horizontal stresses are computed by subtracting the pore water pressure from the total vertical and total horizontal stress data shown in Fig. 4a. Fig. 5a illustrates the evolution of both effective stresses over time. During the first 100 days following the commencement of construction, the effective stresses remained near zero. This suggests that the initial condition of the peat was extremely soft, essentially acting as a fluid. During this time, the contractor had no choice but to perform continuous filling until the embankment height was effectively above the original ground level; without this, the ground would have continued to settle without achieving an initial effective embankment stress. After 100 days, both effective stresses increase linearly with time, indicating the dissipation of excess pore water pressure as the peat solids move into inter-particle contact, thereby consolidating and gaining shear strength. Overall, the excess pore water pressure generated by external loading remains low, with the pore pressure ratio consistently falling well below 30% and remaining under 10% for the majority of the monitoring period (Fig. 5b). This suggests that the peat undergoes relatively rapid consolidation through efficient excess pore water pressure dissipation. Fig. 5c presents the evolution of K_{mob} over time, as determined using Equation 1. It includes the lateral earth pressure coefficients K_o, K_a and K_p, which are calculated using the following equations:

$$K_o = 1 - \sin\varphi' \quad (2)$$

$$K_a = \frac{1 - \sin\varphi'}{1 + \sin\varphi'} \quad (3)$$

$$K_p = \frac{1}{K_a} \quad (4)$$

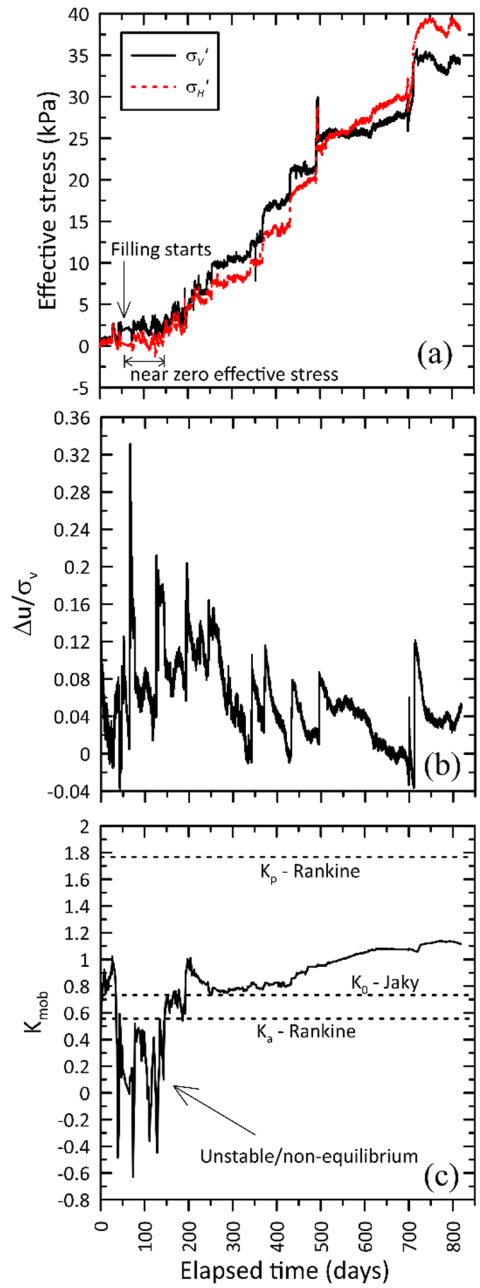

Fig. 5. Evolution of effective stresses and K_{mob} (a) effective stress vs. elapsed time, (b) excess pore water pressure to total vertical stress ratio vs. elapsed time, (c) K_{mob} vs. elapsed time.

The at-rest earth pressure coefficient K_o is determined using Jaky's equation for normally consolidated soil, while K_a and K_p represent the Rankine active and passive lateral earth pressure coefficients, respectively. Based on the peat internal friction angle ϕ' = 16.1°, the calculated values for K_o, K_a, and K_p are 0.72, 0.57, and 1.77, respectively. The K_a and K_p values define the lower and upper boundaries (limiting stress states) for the absolute minimum and maximum horizontal pressures a soil mass can exert in a state of plastic equilibrium. Values falling outside these limiting states may indicate a state of shear failure or lateral flow.

Prior to initial filling, K_{mob} remains at the K_o state. However, at the onset of construction, K_{mob} drops below the K_a limit and fluctuates erratically until Day 150. This period of instability coincides with the duration of near-zero effective stress observed in Fig. 5a. Consequently, the states recorded below K_a represent a condition where the peat possesses negligible effective stress, essentially behaving as a heavy fluid rather than a structured solid mass.

As the effective stress within the peat increases, K_{mob} rises to values between K_a and K_o. This condition persists for approximately 50 days, representing a stage where the soil has reached equilibrium and begun to gain shear strength, while remaining in a relatively loose, partially consolidated state. Subsequently, K_{mob} continues to increase toward values between K_o and K_p, indicating that the peat is becoming more squeezed laterally. However, at the current stage, the K_p limit has not yet been reached; instead, K_{mob} has begun to plateau, showing only a marginal increase at a value of approximately 1.1.

Fig. 6 illustrates the relationship between vertical and lateral strains versus K_{mob} for the peat layer. Strains are defined as the vertical deformation (δV) or horizontal displacement (δH) normalized by the initial peat thickness (H_{peat}). The results indicate that unstable/non-equilibrium conditions occur when strains remain below 5%. The 5% of strain provides critical construction window, where the site is at its most vulnerable and cannot support rapid loading. This level of strain is considered negligible, implying that no significant settlement is perceptible during the unstable construction phase. However, as compression continues, K_{mob} values increase rapidly toward the K_p limit. This is particularly evident under lateral compression, where a K_{mob} value of 1.1 currently corresponds to a horizontal strain of 9% and a vertical strain of 35%.

As the peat undergoes an increasing lateral compression (squeezing), calculating the proximity of K_{mob} to K_p is essential for determining how closely the soil approaches its upper limit, where the failure state occurs. Historically, peat failure in the passive state manifests as shearing, heaving, or lateral bulging. To quantify the proximity to such failure, specifically the stability against lateral squeezing, this study proposes a mobilization ratio approach.

The mobilization ratio is defined herein as the ratio of the current mobilized stress state to the available passive resistance:

$$R_{mob} = \frac{K_{mob} - K_o}{K_p - K_o} \times 100\% \tag{5}$$

The mobilization ratio (R_{mob}) defined in Equation (5) normalizes K_{mob} between K_o and K_p, providing a quantitative estimate of stability before lateral squeezing occurs. This type of instability can theoretically manifest even if significant effective stress gain has already been achieved. According to this formulation, instability against lateral squeezing (passive failure) potentially occurs as R_{mob} approaches 100%. Based on Equation (5), the peat has currently mobilized 36% of its passive capacity, leaving a 64% reserve before reaching the failure threshold. While the embankment is considered stable with this 64% margin, the current state necessitates engineering caution. Note that the 36% mobilization value represents the estimate at the conclusion of the current filling stage. The increase of K_{mob} toward K_p serves as an indicator of the soil mobilizing its shear resistance. This allows the engineer to predict when the next filling stage can safely begin . If the slope of K_{mob} flattens (plateaus) within the limits, it suggests the soil has achieved a stable configuration.

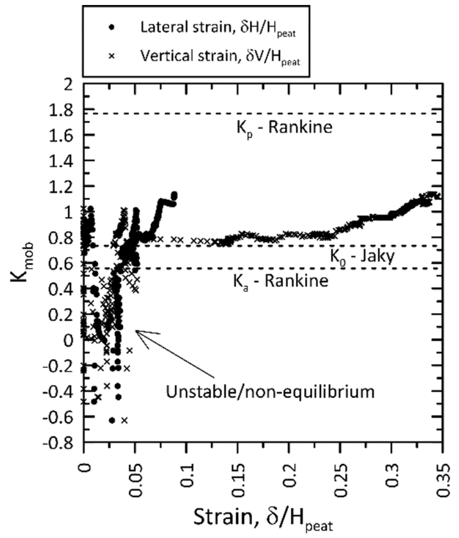

Fig. 6. K_{mob} vs. peat deformations

In many geotechnical contexts, the vertical effective stress (σ_v') at the centerline of a symmetrical embankment is assumed to be the major principal effective stress (σ_1), while the horizontal effective stress (σ_h') represents the minor principal stress (σ_3). This assumption holds true only if the soil remains laterally confined. However, field data reveals a horizontal strain of up to 9% at the centerline, contradicting the standard K_o assumption. While ideal geometry might suggest zero lateral displacement, the inclinometer data suggests the peat is not undergoing pure one-dimensional K_o consolidation. Unlike a perfectly confined oedometer test, the peat under the embankment is moving laterally, i.e. one dimension vs. two dimensions. This lack of confinement implies that the peat is experiencing lateral squeezing and principal stress rotation. Consequently, these lateral movements can lead to higher-than-expected settlement and a reduced factor of safety against bearing capacity failure.

In order to evaluate the evolution of lateral earth coefficients across varying stress states during staged embankment loading, a stress path approach is adopted, utilizing mean effective stress (p') versus deviatoric stress (q). It is noted that p' and q are theoretically, functions of the principal stresses (σ_1 and σ_3). However, in the absence of measurable shear stress data on the vertical and horizontal planes (τ_{vh}), σ_v' and σ_h' are utilized as nominal substitutes. In situ monitoring typically lacks the capability to measure the shear stress component (τ_{vh}) necessary to compute the exact principal stresses (σ_1 and σ_3). Consequently, σ_v' and σ_h' serve as the most reliable indicators of the in-situ stress state for this analysis. Given the observed 9% lateral strain, it is recognized that principal stress rotation is occurring; therefore, the calculated stress path represents a lower-bound estimate of the actual shear mobilization within the peat layer.

Table 3. Summary of the evolution of the K_{mob} during staged embankment loading.

Phase	Duration (days)	Strain range	K_{mob} behavior	Engineering Significance
Initial/Fluid	0-150	0-5%	Erratic ($K_{mob} < K_a$)	High risk; soil behaves as a slurry
Stabilization	150-200	5-10%	$K_a < K_{mob} < K_o$	Shear strength gain begins; Stable consolidation
Lateral Squeezing	200-present	10-35%	$K_a < K_{mob} < 1.1$	Approaching passive resistance

Fig. 7 illustrates the stress path for the peat layer, where the mean effective stress (p') and deviatoric stress (q) are calculated as follows:

$$p' = \frac{\sigma_v' + 2\sigma_h'}{3}; \quad q = \sigma_v' - \sigma_h' \tag{6}$$

To further characterize the stress state, the 1D oedometric K_o-compression line and the theoretical failure envelopes are incorporated into the analysis. These envelopes define the upper limit (active, compression) and the lower limit (passive, extension), providing a reference framework to identify the proximity of the peat to a failure state. The slopes for the K_o-compression line (M_{Ko}), the compression failure line/envelope (M_{comp}), and the extension failure line/envelope (M_{ext}) are derived as follows:

$$M_{Ko} = \frac{3(1 - K_o)}{1 + 2K_o} \tag{7}$$

$$M_{comp} = \frac{6 \sin\varphi'}{3 - \sin\varphi'} \tag{8}$$

$$M_{ext} = \frac{6 \sin\varphi'}{3 + \sin\varphi'} \tag{9}$$

Using the peat internal friction angle $\phi' = 16.1°$, the $M_{Ko} = 0.24$, the $M_{comp} = 0.61$, and the $M_{ext} = 0.51$.

As illustrated in Fig. 7, the stress path initially exhibits non-equilibrium readings, with data points plotting above the compression failure envelope as a result of the initial instabilities discussed in previous sections. Following this initial phase, the peat begins to consolidate, with the stress path approximating the K_o consolidation line until the mean effective stress (p') reaches approximately 15 kPa. During this stage, the deviatoric stress (q) would likely coincide with the K_o line if the induced shear stresses were fully accounted for.

When $p' > 15$ kPa, the stress path deviates significantly from the K_o-compression line as the peat enters a phase of passive loading. This phase is characterized by a rapid increase in horizontal effective stress (σ_h') relative to vertical stress (σ_v'). At approximately $p' = 25$ kPa, the major and minor stresses undergo a reversal, where σ_h' becomes the major stress. Although this passive loading continues, the final stress state remains well within the stable region and is safely distanced from the extension failure envelope.

The field data and analysis demonstrate that geometric symmetry does not guarantee stress symmetry. Despite the symmetrical design of the embankment, the sequential loading of one side induced a horizontal thrust that subsequent filling on the opposing side could not neutralize, a phenomenon clearly captured by the inclinometer data. This emphasizes the necessity of monitoring lateral displacement even at the centerline, as construction sequencing can induce unexpected shear stresses that invalidate the K_o consolidation assumption.

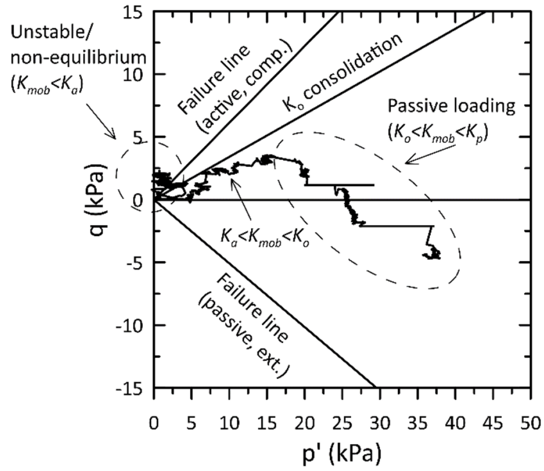

Fig. 7. Stress path.

Conventional design assumptions based on one-dimensional consolidation (oedometer) tests likely underestimate the lateral flow inherent in soft peat. A vertical stress path (increasing q with constant p') would signal a dangerous undrained condition; however, the migration of the path toward $p' = 25$kPa confirms that the peat is gaining effective strength through successful pore water pressure dissipation and densification.

Post-stress reversal (i.e., $p' > 25$kPa), the peat is primarily compressed horizontally by the side-fills rather than vertically. This shift in the stress state requires engineers to look beyond vertical settlement and account for lateral squeezing, which can transition the failure mode from active sliding to passive heaving. Consequently, these insights allow for the optimization of counterberms. While the stress path, q (as in Fig. 7) approach provides a useful nominal stress path, the significant 9% lateral strain implies that the true shear stress is higher than plotted, meaning the soil is closer to the failure envelope than the simplified calculation suggests.

6 Conclusions

This study examines the development of the K_{mob} coefficient based on field observations, focusing on its behavior throughout the sequential loading stages of embankment development. The following conclusions can be drawn:

1. Contrary to the common assumption that K_{mob} remains bounded between K_a and K_p, this study reveals that K_{mob} begins in an unstable state ($K_{mob}<K_a$), evolves through K_a and K_o, and ultimately trends toward K_p. The phases, durations, strains, and behavioural significance of this evolution are summarized in Table 3.

2. Inclinometer data confirms that the peat does not undergo pure one-dimensional oedometric K_o compression/compression. Despite the centerline symmetry of the embankment geometry, the soil experiences measurable lateral strain, which contributes to the observed settlement. While the peat trends toward the K_o-compression/consolidation line as effective stress increases, this study demonstrates that K_{mob} follows a unique evolution dictated by the material's stress path, traversing the range from K_a to K_o.
3. If the consolidation processes are carefully controlled, the material proceeds from K_o-compression/consolidation to undergo compression under a passive loading state, with K_{mob} transitioning toward K_p.
4. Monitoring K_{mob} serves as a critical real-time indicator for maintaining embankment stability during construction, offering a proactive approach to site management. This tracking enables the precise optimization of construction protocols by refining filling sequences and rest periods, which significantly enhances operational efficiency and accelerates project timelines. While these initial results are highly promising, the authors are committed to further solidifying this framework through ongoing validation. To that end, extended analyses are already being conducted across additional field test sites, ensuring that this innovative analytical framework is robustly confirmed for a diverse range of geotechnical and field conditions.
5. The integration of stress sensors with standard instrumentation, such as settlement plates, extensometers, and inclinometers, provides the high-fidelity data essential for rigorous geotechnical analysis. This multi-parameter monitoring approach equips field engineers with the real-time insights necessary to optimize construction management and ensure the stability of embankments on soft ground.

The authors acknowledge the financial and technical support of the Public Works Department (JKR) Sarawak under research grant No. RG/F02/JKRS/02/2021, registered with Universiti Malaysia Sarawak (UNIMAS). We also thank the consultants, contractors, and field personnel for their cooperation during the instrumentation program.

References

1. P. Kissane, F.J. Buggy, G. Ward, B.A. McCabe, F.F. Masrour, F. Towey, Staged construction of surcharged embankments over peat for a national road in Co. Donegal, Ireland, in Proceedings of the XVIII ECSMGE 2024, 2388–2393 (2024). https://doi.org/10.1201/9781003431749-458
2. G. Mesri, M. Ajlouni, Engineering Properties of Fibrous Peats. J. Geotech. Geoenviron. Eng., ASCE. **133**:7(850) (2007). https://doi.org/10.1061/(ASCE)1090-0241(2007)133:7(850)
3. G.W Clough, J.M. Duncan, Finite element analyses of retaining wall behavior. J. Soil Mech. Found. Div., ASCE, **97**, 12 (1971).
4. O' Kelly, Measurement, interpretation and recommended use of laboratory strength properties of fibrous peat, ICE Geotech. Res., **4**, 3, 136–171(2017) http://dx.doi.org/10.1680/jgere.17.00006
5. T.B. Edil, A.W. Dhowian, At-rest lateral pressure of peat soils, J. Soil Mech. Found. Div., ASCE, **107**, 2, 201–217, (1981).
6. J.M. Duncan, R.B. Seed, Compaction-induced earth pressures under K_0-conditions. J. Geotech. Geoenviron. Eng., ASCE, **112**, 1 (1986).
7. D. Perozzi, A.M. Puzrin, Experimental Study of the Earth Pressure Evolution on a Model Wall Rotating about Its Base. J. Geotech. Geoenviron. Eng., ASCE, 150, 7, (2024). https://doi.org/10.1061/JGGEFK.GTENG-12163
8. L. von Post, E. Granlund, E., Södra Sveriges torvtillgångar I [Peat resources of Southern Sweden I]. Sveriges Geologiska Undersökning (SGU), Series C, No. 335. (1926)
9. ASTM, Standard Classification of Peat Samples by Laboratory Testing, West Conshohocken, D4427 (2018) https://doi.org/10.1520/D4427-18
10. Soil Survey Staff. (2022). Keys to Soil Taxonomy (13th ed.). U.S. Department of Agriculture, Natural Resources Conservation Service. https://www.nrcs.usda.gov/resources/guides-and-instructions/keys-to-soil-taxonomy (2022)
11. G.W. Mankinen, B. Gelfer, Commercial peat production in New Brunswick, in Proceedings of the 6th International Peat Congress, Duluth, MN, 534–540, (1982)
12. B.B. Huat,A. Prashad, A. Asadi, S. Kazemian, Geotechnics of Organic Soils and Peat. CRC Press., (2014).
13. A. Hasan, J. Tay, J. Lee, In-Peat Geomechanical Monitoring Method under Actual Road Embankment, Indones. Geotech. J., **2**, 3, 85-94. (2023) DOI: https://doi.org/10.56144/igj.v2i3.64
14. A. Hasan, W.J. Ngelambai, Permeability Behavior of Tropical Sapric Peat under Isotropic Compression, Geotech. Geol. Eng., **42**, 1529-1539 (2024). https://doi.org/10.1007/s10706-023-02612-4